NUCL SCI TECH (2016) 27:30
DOI 10.1007/s41365-016-0027-4

The corrosion of AA2037 aluminum alloy in alkaline aqueous solution studied using slow positron beam spectroscopy

Jiao-Jiao Wang[1] · Zhe-Jie Zhu[1] · Wei Yang[1] · Yi-Chu Wu[1] · Tong-Guang Zhai[2]

Received: 25 April 2015 / Revised: 23 July 2015 / Accepted: 1 August 2015 / Published online: 6 April 2016

Abstract Corrosion behavior of AA2037 T8 Al alloy in a 1 M NaOH aqueous solution was investigated using slow positron beam, together with microscopy techniques and electrochemical tests. The alloy was homogenized at 510 °C for 2 h and 30 s, respectively, before final peak aging, so that one Sample A had more dispersoids than Sample B after homogenization. It was found that *S* parameter of the Doppler-broadened annihilation was significantly decreased near the surface in both samples in the alkaline solution. With increasing the dissolution time, Sample A showed a slower decrease rate than Sample B, which might imply that the preexistence of more dispersoids might hinder the corrosion process in Sample A. Scanning electron microscopy and atomic force microscopy observations found that the surfaces of both samples were uniformly thinned due to intense chemical dissolution by the attack of OH^-. With increasing the dissolution time, Sample B was corroded more substantially and produced more and larger pits in a short dissolution time than Sample A. Furthermore, polarization curves showed that Sample A had a lower corrosion current and corrosion rate than Sample B, which revealed that the presence of the dispersoids was responsible for the better corrosion resistance in the alloy.

✉ Yi-Chu Wu
ycwu@whu.edu.cn

[1] Hubei Key Laboratory of Nuclear Solid Physics, School of Physics and Technology, Wuhan University, Wuhan 430072, China

[2] Chemical and Materials Engineering Department, University of Kentucky, Lexington, KY 40506-0046, USA

Keywords Positron annihilation · Corrosion · Microstructure · Aluminum alloy

1 Introduction

Aluminum alloys are extensively used in aircraft industry because of their high strength, low density, high damage tolerance, and resistance to fatigue crack propagation. Nevertheless, properties of Al alloys in service can be weakened by different types of corrosion, such as intergranular corrosion, pitting corrosion, exfoliation corrosion, and stress corrosion cracking. Aluminum is chemically active and easily oxidized in air. The dense layer of alumina prevents aluminum alloy from further oxidation, hence its excellent corrosion resistance in air. However, the oxide film on aluminum alloy surface dissolves once exposed to acid or alkaline solution, resulting in corrosion damage in the aluminum alloy [1, 2]. Corrosion of aluminum alloys has been studied for many years because of its scientific and technological importance [3–5]. Most of the studies are focused on acid or Cl^- ions aqueous corrosion [6–9], and less of them on alkaline solution [10–12]. Defects and precipitates/dispersoids in aluminum alloys play an important role in the process of corrosion. However, the corrosion effects have not been fully understood.

Positron annihilation spectroscopy (PAS) is a sensitive tool for detecting the properties of vacancy-type defects in metals and alloys [13]. The vacancies and other defects produced by heat treatments and quenching in aluminum and aluminum alloys can be well characterized using PAS [14]. Slow positron beam spectroscopy can be used for probing the depth profile of defects in solids and is particularly suitable for analyzing surface and interfacial

defects [15]. The investigation of interfacial defects induced by corrosion in aluminum using PAS was reported by Hebert et al. [16–18], showing that a significant number of defects could be produced at the interface between the Al matrix and surface oxide film due to the dissolution of alumina film in an alkaline or acidic solution. Scanning electron microscopy (SEM) and atomic force microscopy (AFM) confirmed that the cavities were interfacial voids formed along with the voids detected by PAS [19]. Wu et al. investigated corrosion-related microstructure and defects in iron, AISI 304, and 316 stainless steels by positron lifetime and Doppler broadening measurements [20, 21]. An evident increase in the positron response was observed in iron, which was attributed to the production of defects and voids during the initial process of corrosion. However, a significant decrease in the positron response in AISI 304 and 316 SS was found, possibly due to the dissolution of the surface-passivating oxide film during corrosion.

Recently, AA2037 aluminum alloy was successfully produced by a Hazzellet continuous caster. Aluminum alloy plates produced by this method present cost-savings of about 25 % over the conventional direct chill cast method [22]. Vacancy–solute interaction and precipitates of hot bands of continuous-cast AA2037 aluminum alloy after high-temperature annealing and/or artificial aging were studied by PAS [23, 24]. The results indicated that a significant number of nano-sized precipitates (T phase) could be formed at high-temperature annealing, and longer annealing time resulted in the formation of more T phase. A comparative study of corrosion between pure aluminum and aluminum alloy in 1 M NaOH aqueous solution by using the slow positron beam technique was investigated [25], and it was found that the line-width parameter of Doppler-broadened annihilation increased near the surface of pure aluminum after corrosion, while a decrease in the line-width parameter was observed in AA2037 aluminum alloy after corrosion. Corrosion of the alloy needs to be studied under different high temperatures of annealing.

In this work, special attention was paid to characterization of the corrosion damage in the AA 2037 T8 aluminum alloy with and without a large number of dispersoids by using slow positron beam spectroscopy, AFM and SEM. Corrosion behavior of the alloy was investigated by electrochemical test.

2 Experimental

2.1 Sample preparation and corrosion test

AA2037 T8 aluminum alloy was manufactured using Hazzellet continuous casting method by Aleris International (Uhrichsville, OH, USA). The aluminum alloy contained Cu (1.48 %), Mg (0.45 %), Mn (0.24 %), Si (0.06 %), Zn (0.02 %), and Ti (0.02 %). The hot bands were cut into pieces of 20 mm × 20 mm × 2 mm. Two types of the samples were prepared. Sample A: The as-received hot band was first cold-rolled to 70 % deformation and homogenized at 510 °C for 2 h in air. Then, it was stretched with 3 % deformation and finally aged at 150 °C for 7 days. Some cold-rolled samples were homogenized at 510 °C for 30 s and quenched in ice water, ensuring that premature cooling was minimized. Samples A and B were treated under almost the same condition. There were nano-sized dispersoids in both samples. Sample A by long homogenization time contained a large number of dispersoids, while Sample B by short annealing time only contained very few dispersoids. TEM analysis revealed that the dispersoid composition was $Al_{20}Mn_3Cu_2$, of about 5 nm in size. Coincidence Doppler broadening (CDB) experiment confirmed that there existed Mn and Cu in T phase [24].

Surfaces of both samples were ground and polished, rinsed with alcohol in ultrasonic bath, and dried under cold flowing air. 1 M NaOH aqueous solution was prepared from reagent-grade chemicals and deionized water. The samples were immersed in the solution for different durations (0–2 h) at room temperature. After removal from NaOH solution, the corroded samples were thoroughly washed with distilled water and dried with cold flowing air.

2.2 Sample examination

Slow positron beam Doppler broadening measurements were taken in a vacuum system at 10^{-6} Pa at room temperature in Wuhan University [26]. A slow positron flux was about 5 million per second for 40 mCi ^{22}Na radioactive source, a moderator decay rate of 4 % per day, and a positron energy spread as narrow as 2.0 eV. Moderation efficiency using solid neon as moderator was about 1 %, and monoenergetic beam was in spot size of about Φ5 mm. The positron mean implantation depth Z_m (in nm) can be calculated by

$$Z_m = 40E^{1.6}/\rho_{Al} = 14.8E^{1.6}, \quad (1)$$

where $\rho_{Al} = 2.7$ g cm^{-3} is the density of aluminum alloy and E is the positron energy (in keV).

A high-purity Ge detector was used to measure the energy spectra of gamma photons. The positron implantation energy ranged from 0 to 30 keV. Each annihilation line spectrum consisted of 5×10^5 annihilation events, with a counting rate of 1000 cps at 511 keV. In accordance with the previous work [27], two standard line-shape parameters S and W were calculated to characterize the sample with a relative accuracy of 0.001. The VEPFIT software was used to fit the result of the S parameter as function of energy E.

SEM (SIRION 200, FEI, the Netherlands) was used to examine surface topography of the corroded samples. AFM examination (SHIMADZU, SPM-9500J30) of samples was carried out in air in the direct contact mode.

The open-circuit potentials (OCP) and potentiodynamic polarization curve measurements were taken using a CHI660C system and a three-electrode electrochemical cell. A Pt flake, a saturated calomel electrode (SCE), and the sample were used as the counter electrode, the reference electrode, and the working electrode, respectively. The apparent area of the sample that was exposed to 1 M NaOH solution was 1 cm^2. The potentiodynamic polarization curve was measured at the scan rate of 5 mV/s from −3.1 to −0.1 V potential (referred to as open-circuit potential) after 5-min initial delay. The corrosion current density and corrosion rate were determined by Tafel extrapolation method. All dissolution experiments were performed at room temperature. The corrosion results were averaged from at least measurements of each sample.

3 Results and discussion

3.1 Slow positron beam measurement

The S parameter as a function of positron incident energy E, i.e., $S(E)$ profiles, for Samples A and B at different dissolution durations in 1 M NaOH solution is shown in Fig. 1. According to Eq. (1), the mean implantation depth of positrons from the surface is given on the top axis. The S parameters are normalized to the bulk value ($S = 0.515$), which is approached for $E > 20$ keV. All samples have low S values of 0.92–0.94 close to surface for $E < 2$ keV. For 2 keV $< E <$ 8 keV with larger depths, there was a maximum of S value at which the positrons annihilate in low-momentum valence electrons in interfacial defect layer. For $E > 20$ keV, S approaches a constant value since all positrons are essentially implanted into the matrix before being annihilated. A significant decrease in S parameter is found after dissolution for both samples. The broad peak in $S(E)$ indicates that there exists a near-surface defect layer in both samples after 10 min in 1 M NaOH solution. As dissolution time increases, the peaks weaken gradually and then disappear. The results agree with those of the corrosion of water-quenched Al alloy [25], but both samples changed little after 10-min dissolution as they further deformed to 3 % and aged at 150 °C for 7 days, resulting in the production of many defects and precipitates induced by deformation and/or peak aging.

Comparing the $S(E)$ profiles in Fig. 1a, b, it can be seen that the virgin Sample A has larger S in interfacial defect layer than the virgin Sample B, and after corrosion, the $S(E)$ profiles of both samples decrease, but the decrease rate of Sample A is slower than that of the Sample B.

To learn about defects types for both samples during early stages of corrosion, W parameters as a function of S parameter are shown in Fig. 2. All the coordinate points (S, W) fall on a common locus and distribute near by a straight line, indicating that only two kinds of positron states contribute to the annihilation [28]. Thus, only one type of defect appears in all the measurements. For the original samples, positrons mainly annihilate in interface layer and bulk, while for the corroded samples positrons mainly annihilate in corrosion product in layer and bulk.

To obtain the depth distribution of defects, the VEPFIT program was used to fit the $S(E)$ profiles. The results are plotted as solid lines in Fig. 1. The dissolution rate in NaOH solution was very rapid (which will be discussed in the Sect. 3.3). The initial defect layer was dissolved in a few minutes. After the treatment, the defect layer was

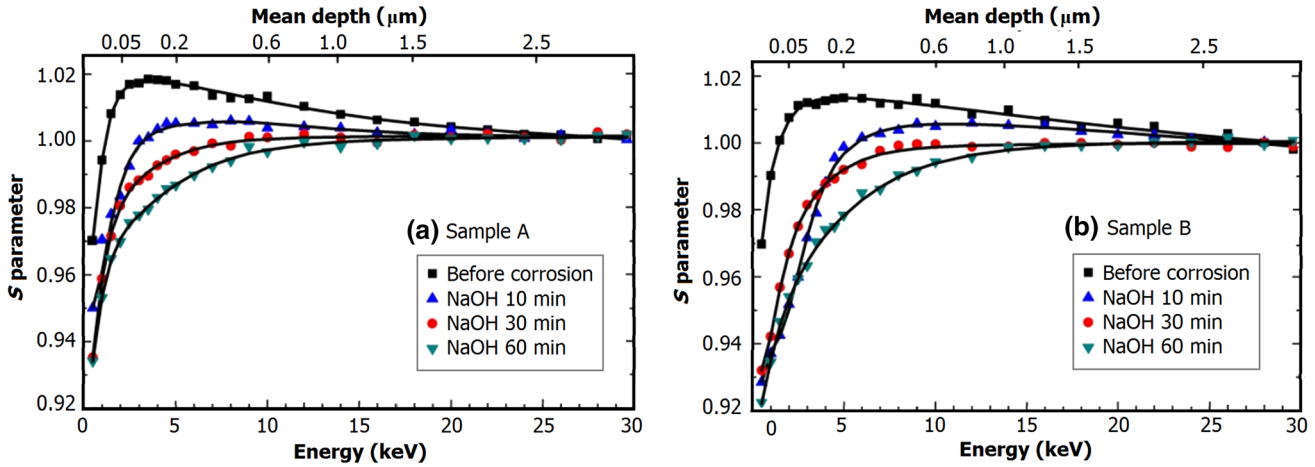

Fig. 1 S parameter as a function of position incident energy and mean depth, for the samples corroded in 1 M NaOH solution for different minutes. The *solid lines* are fits to the data

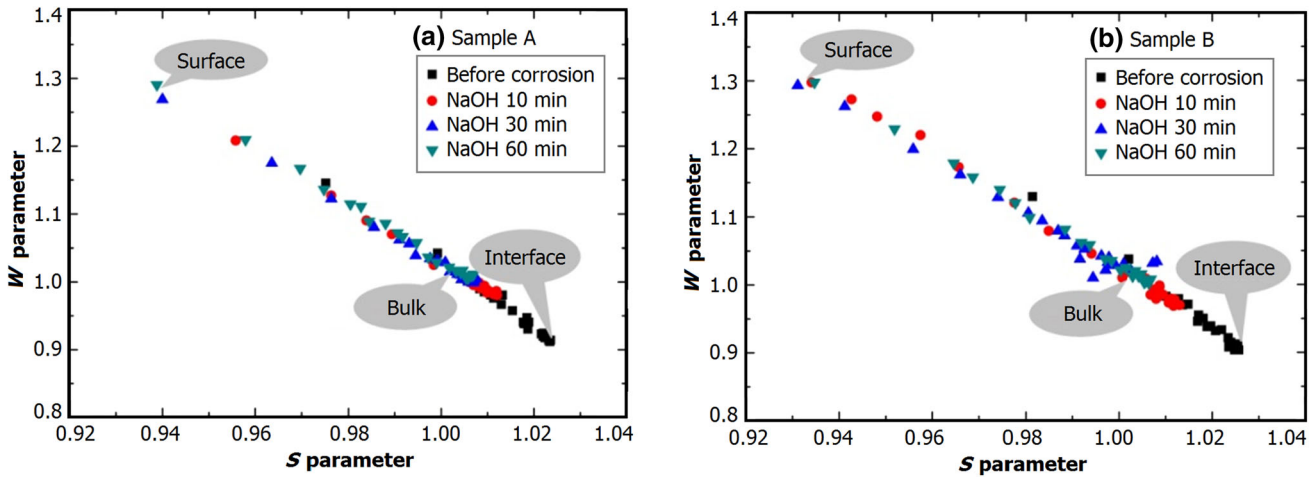

Fig. 2 *W* parameter as a function of *S* parameter of the samples corroded in 1 M NaOH solution for different minutes

replaced by new surface corrosion layer introduced by the dissolution. Therefore, the simple two-layer model (near-surface corrosion layer and bulk), i.e., assuming no interface layer, was employed for the fitting. The positron diffusion length of bulk Al alloys was fixed at about 200 nm as reported for metals and alloys [19, 25]. Table 1 shows the fitted results of the interfacial defect layer (or near-surface corrosion layer) S (S_d), positron diffusion length (L_d), and thickness (B_d). The S_d parameter of defect layer decreases with increasing dissolution time in both samples, and the decrease rate of Sample A (from 1.025 to 0.996) is slower than that of Sample B (from 1.022 to 0.985). L_d of both samples increases after dissolution, but does not change too much with dissolution time, indicating a lower defect/void concentration or the formation of near-surface corrosion layer. The layer thickness B_d is 300–350 nm, which is much longer than that of virgin samples (about 50 nm).

Many experiments [3–5, 25, 29] indicated that Cu affects strongly on corrosion of aluminum alloys. The significant decrease in S parameter observed after the corrosion of AA2037 alloy can be explained by invoking two possible causes: copper enrichment within the metal–oxide interface layer and formation of new corrosion layer. The annealed Cu has a low S value of 0.83 due to the presence of 3d electrons. The content of Cu in AA2037 aluminum alloy is only 1.48 %. Therefore, Cu enrichment near the metal–oxide interface layer shall induce a decrease in the S parameter. The Cu enrichment increases with dissolution time, and thus, the S parameter decreases. In addition, the positron diffusion length increases after NaOH dissolution, indicating the formation of near-surface corrosion layer (i.e., the formation of new oxides or hydroxides). As a result of the preexistence of many dispersoids, the rate of Cu enrichment or corrosion layer formation was slower in Sample A than in Sample B, and so the S parameter decreased less with increasing dissolution time, which implies that the preexistence of a number of dispersoids introduced during homogenization shall hinder the corrosion processes. Additional measurements confirmed that a thick oxide film (a few μm) was formed at the surface of AA2037 aluminum alloy samples after immersion in pure water for several months, resulting in a lower near-surface S parameter. Further investigations are in progress and will be reported in the future.

3.2 Morphology characterization

Figure 3 shows typical SEM surface morphology of Samples A and B after different minutes of exposure to 1 M NaOH solution. Figure 3a, f is the microstructure of the virgin samples, for comparison with the corroded

Table 1 Fit values of the interfacial defect layer S (S_d), positron diffusion length (L_d), and thickness (B_d) for Samples A and B after different dissolution durations (t) in 1 M NaOH solution

t (min)	Sample A			Sample B		
	S_d	L_d (nm)	B_d (nm)	S_d	L_d (nm)	B_d (nm)
0	1.025 ± 0.001	15 ± 1	46 ± 3	1.022 ± 0.001	19 ± 1	55 ± 4
10	1.014 ± 0.001	34 ± 2	315 ± 10	1.010 ± 0.001	61 ± 3	298 ± 8
30	1.003 ± 0.001	35 ± 1	321 ± 9	0.996 ± 0.001	41 ± 2	339 ± 10
60	0.996 ± 0.001	51 ± 3	330 ± 11	0.985 ± 0.001	58 ± 3	340 ± 12

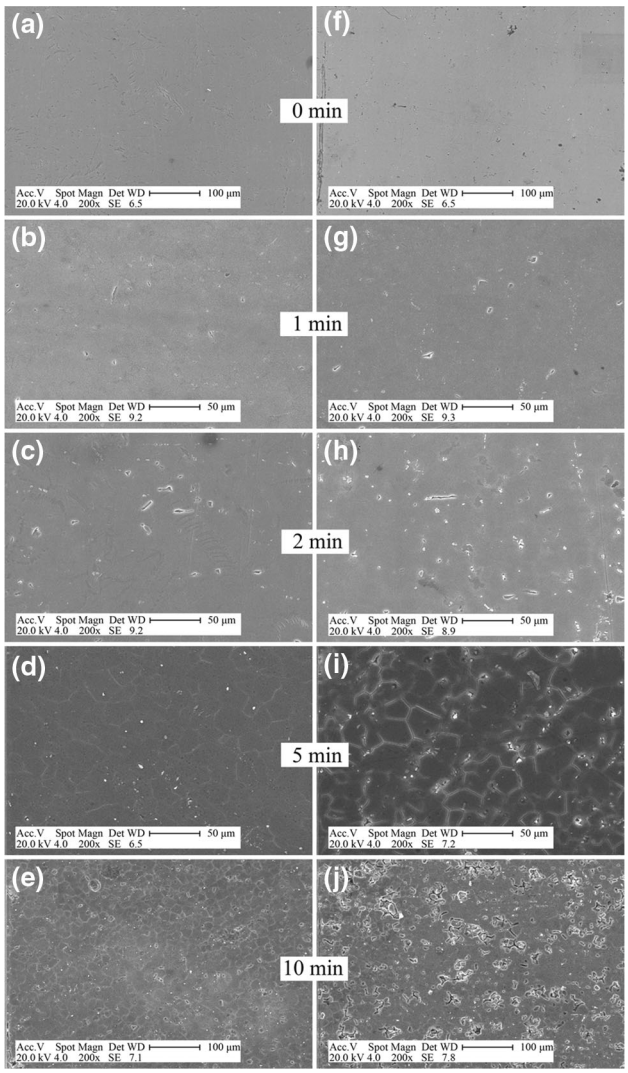

Fig. 3 SEM images of Sample A (**a**–**e**) and Sample B (**f**–**j**) tested in 1 M NaOH solution for different dissolution durations

surfaces. When the samples were immersed in NaOH solutions, high effervescence of the solution surrounding the samples was observed due to the formation of gaseous H_2 [30, 31]. Figure 3b, g shows that the original thin oxide film was dissolved after 1-min immersion by the high OH^- concentration in alkaline solution. Both samples mainly consisted of α-Al matrix with tiny precipitates introduced by peak aging at 150 °C. The precipitates were confirmed to be Cu-containing intermetallics on the alloy surface by corresponding EDS spectrum (not shown). The surface of samples is uniformly thinned by alkaline chemical dissolution, and local corrosion of some grain boundaries or precipitates is facilitated by attack of OH^- from dissolution time of 1 min to 10 min [32]. Compared to the surface morphology of Sample A (Fig. 3b–e), Sample B (Fig. 3g–j) at the same dissolution time (e.g., 5 min) was corroded more seriously, with more flawed regions at a dissolution time of 10 min. This may be because that, introduced during homogenization, Sample A had more dispersoids, which hindered the corrosion processes.

Figure 4 shows AFM images of the corroded surface of the samples. Some cavities on the surface of both samples after immersion for 1 and 2 min are found to be associated with inclusions or large corrosion pits. As shown in Fig. 3, Sample B was corroded more seriously and produced more and larger cavities or microvoids than Sample A. The results support that Sample A has a better resistance to corrosion than Sample B due to the presence of more dispersoids, which is in good agreement with Doppler broadening measurements.

Doppler broadening measurement (Fig. 1) has a resolution around 10^1–10^2 nm in depth and can be used to evaluate the thickness of surface layer or interfacial defect layer without cross-sectioning the sample. This resolution cannot be easily achieved by SEM and AFM (Figs. 3, 4). In characterizing surface layers and near-surface region, slow positron beam technique with such a resolution plays an irreplaceable role. SEM reveals just sample morphology and composition distribution, while the positron beam technique is sensitive to vacancy-type defects and defect's chemical environment that are closely associated with corrosion reactions. In this sense, the positron beam is an essential complement to SEM.

3.3 Analysis of open-circuit potential and polarization curve

Figure 5 shows the open-circuit potential as a function of dissolution time for Samples A and B in 1 M NaOH solution. In these transients, at first the potential decreased dramatically to a minimum in less than 20 s. The initial potential decline is attributed to the dissolution of oxide film on the surface, as a result of its high solubility in the alkaline solution. The potential increased rapidly up to 2 min, and then the increase became slowly. These are in good agreement with open-circuit corrosion of Al in alkaline solutions [33–35]. Based on the mechanism of corrosion of Al in alkaline solutions suggested by Adhikari et al. [35, 36], the value of the minimum potential of electropolished samples indicated that it was determined by the Nernst potential for oxidation of surface AlH_3. The potential increases quickly first and then slowly. The former is attributable to the formation of surface hydride, while the latter is due to the enrichment of Cu impurities on the surface, which anodically polarizes Al by accelerating the cathodic process. Therefore, we suggest that the corrosion mechanism of Al alloy in alkaline media may be related to the buildup of a protective layer of $Al(OH)_3$. The transients of Sample A in Fig. 5 are offset to more negative potential than that of Sample B. This

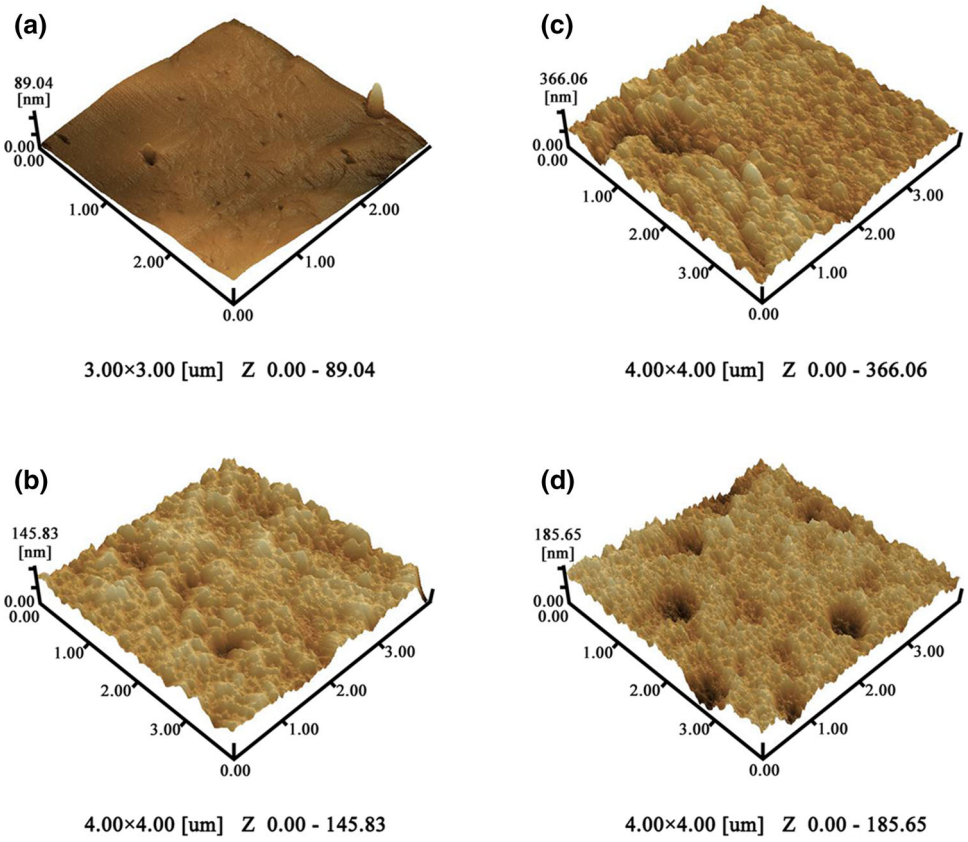

Fig. 4 AFM micrographs of the surface topographies of Samples A after dissolution in 1 M NaOH solution for 1 min (**a**) and 2 min (**b**), and of Sample B after dissolution in 1 M NaOH solution for 1 min (**c**) and 2 min (**d**)

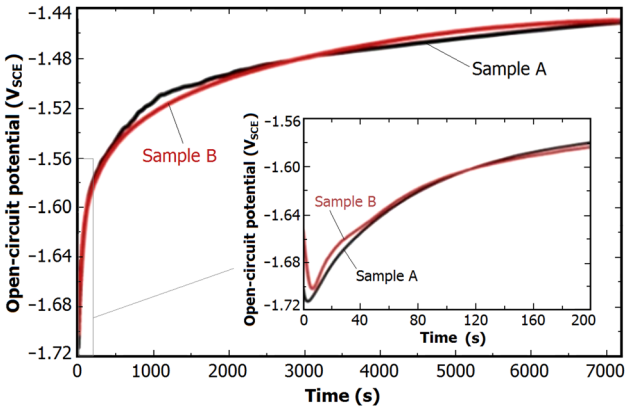

Fig. 5 Comparison of open-circuit potential transients for Samples A and B in 1 M NaOH solution

may be attributable to surface composition changes or microstructure in sample surface layer due to the presence of more dispersoids, which were removed in the first 2 min of dissolution. The dealloying of Cu-containing intermetallics on the alloy surface may occur in long-time immersion. During dealloying, S-phase (Al_2MgCu) [37, 38] intermetallic undergoes selective dissolution (an increase in the elemental Cu on the alloy surface) in NaOH solution, leading to a slow increase in open-circuit potential value.

Figure 6 shows the typical potentiodynamic polarization curves of the samples corroded in 1 M NaOH solution. The polarization curves were used to measure the corrosion current density, i_{corr} at E_{corr}, by Tafel extrapolation of the polarization curve. It can be seen that both anodic and cathodic polarization curves of Sample A are lower than those of Sample B, indicating that the former is

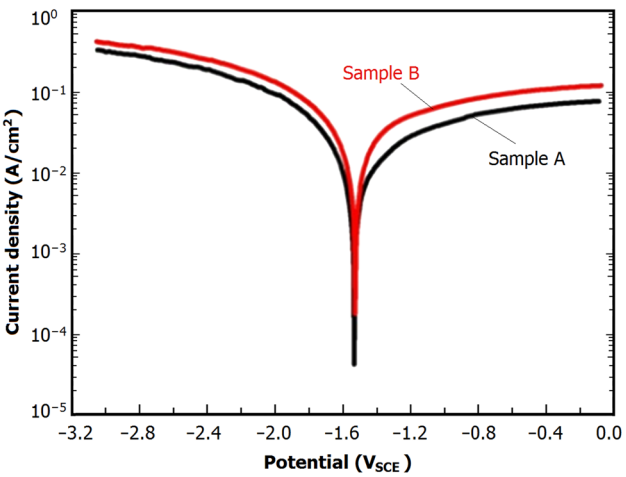

Fig. 6 Polarization curves of Sample A and Sample B in 1 M NaOH solution

Table 2 Corrosion parameters and self-corrosion rate of the studied alloy in 1 M NaOH solution

Samples	Corrosion potential E_{corr} (V)	Corrosion current density i_{corr} (mA cm^{-2})	Corrosion rate	
			d (g m^{-2} h^{-1})	d [mm a^{-1}(nm min^{-1})]
A	−1.532 ± 0.021	10.96 ± 0.62	36.76 ± 0.75	119.5 ± 2.3 (227)
B	−1.524 ± 0.015	16.22 ± 0.95	54.89 ± 0.85	176.8 ± 2.7 (336)

electrochemically less active than the latter. The corrosion rate was calculated using the following equation [39]:

$$\upsilon = \frac{M}{nF} i_{corr} = 3.73 \times 10^{-4} \frac{M}{n} i_{corr}, \quad (2)$$

$$d = \frac{\upsilon}{\rho} = 3.28 \times 10^{-3} \frac{M}{n\rho} i_{corr}, \quad (3)$$

where M is the atomic weight, n is the valence, F is the Faraday constant in C mol^{-1}, i_{corr} is the current density in μA cm^{-2}, v is the corrosion rate in g m^{-2} h^{-1}, ρ is the density in units of g cm^{-3}, and d is the corrosion rate in mm a^{-1}.

The electrochemical parameters of the samples are listed in Table 2. The E_{corr} of both samples are about the same (1.53 and 1.52 V), indicating that they have similar susceptibility to the corrosion initiation. However, the i_{corr} (11.0 mA cm^{-2}) and corrosion rate (119 mm a^{-1}) of Sample A are lower than those of Sample B (16.2 mA cm^{-2} and 176 mm a^{-1}), revealing that Sample A has a better corrosion resistance than Sample B. The results are similar to the data reported by Refs. [32, 40] and are consistent with the results of microstructure analysis and Doppler broadening measurements. In this study, the evaluation of corrosion behavior using the Tafel extrapolation method or the electrochemical technique allows one to determine and understand the difference in tendency to corrode between Samples A and B under the same testing condition.

Corrosion behavior of AA 2037 T8 Al alloys will be further studied with immersion tests in NaCl or acidic aqueous solutions in follow-up studies.

4 Conclusion

Doppler broadening measurements of slow positron beam show that for the original samples without corrosion, Sample A has larger S in interfacial defect layer than Sample B. A significant decrease in S parameter is found after NaOH dissolution for both samples. The broad peak in $S(E)$ indicates that there existed a near-surface defect layer in both samples after short times in 1 M NaOH solution. When the dissolution time increases, the peaks gradually weaken and then disappear due to the formation of corrosion layer. During the dissolution, the decrease rate of S parameter of Sample A is slower than that of the Sample B, which implies that the preexistence of many dispersoids introduced during homogenization will hinder the corrosion processes.

SEM and AFM observations reveal that the original thin oxide film of both samples was dissolved after immersion for 1 min in the presence of high OH^- concentration in alkaline solution. With increasing the dissolution time, the surface of samples is uniformly thinned due to intense chemical dissolution by attack of OH^-. Sample B is corroded more seriously and produces more and larger cavities at short dissolution time than Sample A.

The electrochemical tests show that the initial open-circuit potential decrease is attributable to dissolution of the surface oxide film. The E_{corr} of both samples is about the same, which indicates that they are of similar susceptibility to the corrosion initiation. However, the i_{corr} and corrosion rate of Sample A are smaller than those of Sample B, which reveals that Sample A has a better corrosion resistance than Sample B.

Acknowledgments This work was supported by National Science Foundation (Nos. 11175136, 51071111, and J1210061). T. Zhai was sponsored by the US NSF through a Grant No. DMR-1207115.

References

1. Z. Szklarska-Smialowska, Pitting corrosion of aluminum. Corr. Sci. **41**, 1743–1767 (1999). doi:10.1016/S0010-938X(99)00012-8
2. M. Lashgari, A.M. Malek, Fundamental studies of aluminum corrosion in acidic and basic environments: theoretical predictions and experimental observations. Electrochim. Acta **55**, 5253–5257 (2010). doi:10.1016/j.electacta.2010.04.054
3. L.L. Shreir, R.A. Jarman, G.T. Burstain, Corrosion: metal/environment reactions. Oxford (England) **4**, 44 (1994)
4. Y. Zhang, S.Q. Liang, Athar Javed et al., Effect of pass deformation on microstructure, corrosion and electrochemical properties of aluminum alloy anodes for alkaline aluminum fuel cell applications. Met. Mater. Int. **19**, 555–561 (2013). doi:10.1007/s12540-013-3025-7
5. W.R. Osorio, M.V. Cante, C. Brito et al., A electrochemical behavior of an Al–Fe–Ni alloy affected by nano-sized intermetallic particles. Corrosion **71**, 510–522 (2015). doi:10.5006/1356
6. H.M. Obispo, L.E. Murr, R.M. Arrowood et al., Copper deposition during the corrosion of aluminum alloy 2024 in sodium chloride solutions. J. Mater. Sci. **35**, 3479–3495 (2000). doi:10.1023/A:1004840908494
7. R.L. Cervantes, L.E. Murr, R.M. Arrowood, Copper nucleation and growth during the corrosion of aluminum alloy 2524 in sodium chloride solutions. J. Mater. Sci. **36**, 4079–4088 (2001). doi:10.1023/A:1017975728838

8. B.B. Wang, Z.Y. Wang, W. Han et al., Atmospheric corrosion of aluminium alloy 2024-T3 exposed to salt lake environment in Western China. Corr. Sci. **59**, 63–70 (2012). doi:10.1016/j.corsci.2012.02.015
9. H.W. Shi, Z.H. Tian, T.H. Hu et al., Simulating corrosion of Al_2CuMg phase by measuring ionic currents, chloride concentration and pH. Corr. Sci. **88**, 178–186 (2014). doi:10.1016/j.corsci.2014.07.021
10. M.L. Doche, J.J. Rameau, R. Durand et al., Electrochemical behaviour of aluminium in concentrated NaOH solutions. Corr. Sci. **41**, 805–826 (1999). doi:10.1016/S0010-938X(98)00107-3
11. Y. Liu, M.A. Arenas, S.J. Garcia-Vergara et al., Behaviour of copper during alkaline corrosion of Al–Cu alloys. Corr. Sci. **50**, 1475–1480 (2008). doi:10.1016/j.corsci.2008.01.021
12. Y. Ma, X. Zhou, G.E. Thompson et al., Surface texture formed on AA2099 Al–Li–Cu alloy during alkaline etching. Corr. Sci. **66**, 292–299 (2013). doi:10.1016/j.corsci.2012.09.032
13. A. Dupasquier, G. Kögel, A. Somoza, Studies of light alloys by positron annihilation techniques. Acta Mater. **52**, 4707–4726 (2004). doi:10.1016/j.actamat.2004.07.004
14. B. Klobes, K. Maier, T.E.M. Staab, Natural ageing of Al–Cu–Mg revisited from a local perspective. Mater. Sci. Eng. A **528**, 3253–3260 (2011). doi:10.1016/j.msea.2011.01.002
15. P.J. Schultz, K.G. Lynn, Interaction of positron beams with surfaces, thin films, and interfaces. Rev. Mod. Phys. **60**, 701–779 (1988). doi:10.1103/RevModPhys.60.701
16. K.R. Hebert, T. Gessmann, K.G. Lynn et al., Positron annihilation spectroscopy study of interfacial defects formed by anodic oxidation of aluminum. J. Electrochem. Soc. **151**, B22–B26 (2004). doi:10.1149/1.1631821
17. K.R. Hebert, H. Wu, T. Gessmann et al., Positron annihilation spectroscopy study of interfacial defects formed by dissolution of aluminum in aqueous sodium hydroxide. J. Electrochem. Soc. **148**, B92–B100 (2001). doi:10.1149/1.1341241
18. H. Wu, K.R. Hebert, T. Gessmann et al., Corrosion-related interfacial defects formed by dissolution of aluminum in aqueous phosphoric acid. J. Electrochem. Soc. **149**, B108–B116 (2002). doi:10.1149/1.1455648
19. S. Adhikari, L.S. Chumbley, H. Chen et al., Interfacial voids in aluminum created by aqueous dissolution. Electrochim. Acta **55**, 6093–6100 (2010). doi:10.1016/j.electacta.2010.05.073
20. Y.C. Wu, Y.Q. Chen, B. Wang et al., Slow positron beam study of corrosion-related defects in pure iron. Appl. Surf. Sci. **252**, 3274–3277 (2006). doi:10.1016/j.apsusc.2005.08.050
21. Y.C. Wu, R. Zhang, H. Chen et al., Corrosion of iron and stainless steels studied using slow positron beam technique. Radiat. Phys. Chem. **68**, 599–603 (2003). doi:10.1016/S0969-806X(03)00239-1
22. X.F. Yu, Y.M. Zhao, X.Y. Wen et al., A study of mechanical isotropy of continuous cast and direct chill cast AA5182 Al alloys. Mater. Sci. Eng. A **394**, 376–384 (2005). doi:10.1016/j.msea.2004.11.060
23. S.L. Wu, Y.Q. Chen, Y.C. Wu et al., Positron annihilation study of hot band of a continuous cast AA 2037 Al alloy after annealing. Acta Phys. Sin. **55**, 6129–6135 (2006). **(in Chinese)**
24. P.H. Li, Y.C. Wu, J. Jiang et al., Coincidence Doppler broadening study of the precipitates of a continuous Cast AA2037 Al alloy after annealing and ageing. Phys. Procedia **35**, 28–33 (2012). doi:10.1016/j.phpro.2012.06.006
25. Y.C. Wu, T. Zhai, P.G. Coleman, A Positron annihilation study of corrosion of aluminum and aluminum alloy by NaOH. Metall. Mater. Trans. A **43**, 2823–2831 (2011). doi:10.1007/s11661-011-0806-9
26. Y.C. Wu, Y.Q. Chen, S.L. Wu et al., High moderation efficiency positron beamline. Phys. Status Solidi (C) **4**, 4032–4035 (2007). doi:10.1002/pssc.200675825
27. A. Van Veen, H. Schut, M. Clement et al., VEPFIT applied to depth profiling problems. Appl. Surf. Sci. **85**, 216–224 (1995). doi:10.1016/0169-4332(94)00334-3
28. P. Hautojärvi, C. Corbel, *Positron spectroscopy of defects in metals and semiconductors, Positron spectroscopy of solids*, vol. 5 (IOS Press, Amsterdam, 1995), pp. 3–14. doi:10.1051/jp4:1995101
29. Y. Liu, M.A. Arenas, P. Skeldon et al., Anodic behaviour of a model second phase: Al–20at.%Mg–20at.%Cu. Corr. Sci. **48**, 1225–1248 (2006). doi:10.1016/j.corsci.2005.05.007
30. S.M. Moon, S.I. Pyun, The corrosion of aluminium during cathodic polarization in aqueous solutions. Corr. Sci. **39**, 399–408 (1997). doi:10.1016/S0010-938X(97)83354-9
31. H.Z. Wang, D.Y.C. Leung, M.K.H. Leung et al., A review on hydrogen production using aluminum and aluminum alloys. Renew. Sustain. Energy Rev. **13**, 845–853 (2009). doi:10.1016/j.rser.2008.02.009
32. J. Ma, J. Wen, Q. Li et al., Effects of acidity and alkalinity on corrosion behaviour of Al–Zn–Mg based anode alloy. J. Power Sources **226**, 156–161 (2013). doi:10.1016/j.jpowsour.2012.10.075
33. I. Boukerche, S. Djerad, L. Benmansour et al., Degradability of aluminum in acidic and alkaline solutions. Corr. Sci. **78**, 343–352 (2014). doi:10.1016/j.corsci.2013.10.019
34. K.R. Hebert, G. Zhang, K.-M. Ho et al., Modeling electrochemical and metal-phase processes during alkaline aluminum corrosion. Electrochim. Acta **58**, 203–208 (2011). doi:10.1016/j.electacta.2011.09.045
35. S. Adhikari, K.R. Hebert, Factors controlling the time evolution of the corrosion potential of aluminum in alkaline solutions. Corr. Sci. **50**, 1414–1421 (2008). doi:10.1016/j.corsci.2008.01.001
36. S. Adhikari, J. Lee, K.R. Hebert, Formation of aluminum hydride during alkaline dissolution of aluminum. J. Electrochem. Soc. **155**, C16–C21 (2008). doi:10.1149/1.2800770
37. W. Zhang, G.S. Frankel, Transitions between pitting and intergranular corrosion in AA2024. Electrochim. Acta **48**, 1193–1210 (2003). doi:10.1016/S0013-4686(02)00828-9
38. H. Kamoutsi, G.N. Haidemenopoulos, V. Bontozoglou et al., Effect of prior deformation and heat treatment on the corrosion-induced hydrogen trapping in aluminium alloy 2024. Corr. Sci. **80**, 139–142 (2014). doi:10.1016/j.corsci.2013.11.021
39. J. Zhang, M. Klasky, B.C. Letellier, The aluminum chemistry and corrosion in alkaline solutions. J. Nucl. Mater. **384**, 175–189 (2009). doi:10.1016/j.jnucmat.2008.11.009
40. N. Chaubey, Vinod Kumar Singh, Savita et al., Corrosion inhibition of aluminium alloy in alkaline media by Neolamarkia Cadamba Bark extract as a green inhibitor. Int. J. Electrochem. Sci. **10**, 504–518 (2015)